Journal of Food and Drug Analysis

Volume 30
Issue 4 *Special Issue*

Article 7

Simple and rapid detection of ractopamine in pork with comparison of LSPR and LFIA sensors

Recommended Citation
Lee, Min Ji; Aliya, Sheik; Lee, Eun-Seon; Jeon, Tae-Joon; Oh, Mi-Hwa; and Huh, Yun Suk (2022) "Simple and rapid detection of ractopamine in pork with comparison of LSPR and LFIA sensors," *Journal of Food and Drug Analysis*: Vol. 30 : Iss. 4 , Article 7.
Available at: https://doi.org/10.38212/2224-6614.3410

ORIGINAL ARTICLE

Simple and rapid detection of ractopamine in pork with comparison of LSPR and LFIA sensors

Min Ji Lee [a], Sheik Aliya [a], Eun-Seon Lee [c], Tae-Joon Jeon [a,b,*], Mi-Hwa Oh [c,**], Yun Suk Huh [a,b,***]

[a] Department of Biological Science and Bioengineering, Inha University, Incheon 22212, Republic of Korea
[b] Department of Biological Engineering, Inha University, Incheon 22212, Republic of Korea
[c] National Institute of Animal Science, Rural Development Administration, Wanju 55365, Republic of Korea

Abstract

This study developed a simple and rapid strategic technique to detect ractopamine (chemical growth-promoting agent) in pork. Two highly sensitive and specific gold nanoparticle-based portable sensors, i.e., localized surface plasmon resonance (LSPR) sensors, and lateral flow immunoassay (LFIA) strips were developed to detect veterinary drug residues in food products, that have detrimental effects on humans. Optimization studies were conducted on several sensor devices to improve sensitivity. Each sensor comprised functionalized gold nanoparticles conjugated with ractopamine antibodies. The LSPR sensor chip achieved excellent detection sensitivity = 1.19 fg/mL and was advantageous for quantitative analysis due to its wide dynamic range. On the other hand, LFIA strips provided visual test confirmation and achieved 2.27 ng/mL detection sensitivity, significantly less sensitive than LSPR. The complementary sensors help overcome each other's shortcomings with both the techniques offering ease of use, affordability and rapid diagnosis. Thus, these sensors can be applied on-site for routine screening of harmful drug residues in pork meat. They also provide useful direction for advanced technologies to enhance assay performance for detecting various other food drug contaminants.

Keywords: Biosensors, Lateral flow immunoassay, Localized surface plasmon resonance, Ractopamine, Veterinary drugs

1. Introduction

Population, economic growth, and rising income in developing and developed countries have greatly increased the demand for food products [1]. Meat consumption has risen approximately 58% over the past 20 years (1998–2018) and is expected to keep rising [2]. Thus, meat producers have been forced to administer chemical additives and supplements, such as antibiotics, hormones, anti-inflammatories, and β-agonists to improve growth efficiency and meat quality [3]. This has led to increased veterinary drug market growth, which is posing a major threat from misuse and abuse. Administered drug remnants and related metabolites have been found in meat and soil, creating a serious menace for both humans and the environment [4–6]. Human consumption of intended drug contaminated food products poses multiple health hazards, including carcinogenic effects, endocrine malfunction, and allergic reactions [7]. International organizations, such as Codex Alimentarius Commission (CODEX) and European Commission (EU), regulate animal drug usage in the food industry by stipulating maximum residue limits (MRLs) for veterinary drugs [8].

People worldwide have become highly health-conscious and their desire to consume high-quality, healthy, and safe (chemical pesticide-free) food [9], urges developing sensor technology to quickly determine baleful food components in the field to ensure food safety for consumers. Lateral flow assays (LFAs) are recommended for food testing over traditionally more precise methods, such as high-performance liquid chromatography (HPLC) or liquid chromatography-mass spectrometry (LC-MS)

Received 10 January 2022; revised 23 March 2022; accepted 25 March 2022.
Available online 23 November 2022
* Corresponding author at: Department of Biological Science and Bioengineering, Inha University, Incheon 22212, Republic of Korea.
** Corresponding author.
*** Corresponding author at: Department of Biological Science and Bioengineering, Inha University, Incheon 22212, Republic of Korea.
E-mail addresses: tjjeon@inha.ac.kr (T.-J. Jeon), moh@korea.kr (M.-H. Oh), yunsuk.huh@inha.ac.kr (Y.S. Huh).

https://doi.org/10.38212/2224-6614.3410

to analyze veterinary drug residues [10,11], or chromatography-mass spectrometry (GC−MS) [12] and enzyme-linked immunosorbent assay (ELISA) [13]. Although these are highly sensitive and selective methods, they are also time-consuming, and require costly equipment and skilled professionals, limiting on-site applications [14−16]. On the other hand, LFA is relatively easy, convenient, and cost-effective, and consequently has been employed across a wide range of applications covering health monitoring, veterinary fieldwork, environmental testing, agricultural goods, etc. [17]. Lateral flow assays are a mature technology, and well-proven for maintaining assay quality, sensitivity, specificity, reproducibility, and stability for mass production and market acceptance.

The sensor-based LFA has wide applications with more advantages. In the recent decades, the rapid growth of field-enabled sensor technology, colloidal gold nanoparticles (AuNPs) properties such as the small size, excellent optical and material properties, stability, and high surface area makes them suitable candidates. Another main advantage is the synthesis methods are well-established for size control gold nanoparticles based sensing technology [18,19]. Lateral flow biosensors with colloidal AuNPs detect analytes such as proteins, nucleic acids, heavy metals, pesticides, chemical and biological agents at very low concentrations with high biocompatibility and affinity for biomolecule conjugates [20]. Thus, simple, sensitive, and easily applied localized surface plasmon resonance (LSPR) based platforms and lateral flow immunoassay (LFIA) strips are very attractive tools in the field [21]. AuNPs based LSPR sensors can easily detect signals in real-time through spectral shifts and help miniaturize assay platforms because highly localized sensing is possible. Since LSPR based sensors can be very sensitive and specific, they have been widely applied as biosensors in fields such as disease diagnosis; and environmental, food, and agricultural safety monitoring [22−25].

Lateral flow immunoassay strips are the most widely used biosensor worldwide due to their speed, simplicity, and low cost. It is also highly user-friendly, allowing direct visual checks without requiring additional equipment [26,27]. The present study targeted ractopamine as an model for veterinary drugs to confirm detection performance for the developed sensors. Ractopamine promotes pork leanness but has been banned in many countries due to drastic health and behavioral problems in animals [28]. We also checked whether sensing efficiency met USFDA ractopamine residual tolerance criteria (pork muscle: 0.05 ug/mL) [29], using the standard solution and spiked pork sample. Cross-comparison quantitative and qualitative analyses using portable sensor devices were used to assess field application, and we consequently proposed a new food safety detection system incorporating two sensor formats for rapid diagnosis of animal drugs in food.

2. Materials and methods

2.1. Reagents and materials

Gold (III) chloride trihydrate (HAuCl4, ≥99.9%), (3-Aminopropyl) triethoxysilane (APTES, ≥98.0%), and ractopamine hydrochloride were purchased from Sigma−Aldrich (St. Louis, MO, USA). Trisodium citrate dihydrate was purchased from Kanto Chemical Co., Inc. (Tokyo, Japan). Anti-ractopamine monoclonal antibody (RAC-Ab) produced in mice and ractopamine-BSA were purchased from Creative Diagnostics (New York City, NY, USA). All other chemicals used were analytical grade. The absorbent pad, backing card, nitrocellulose membrane, sample pad, and conjugation pad used to fabricate LFIA strips, were purchased from Bore Da Biotech Co. Ltd. (Seongnam, Korea).

2.2. Uniformly sized gold nanoparticle synthesis

Two differently sized gold nanoparticles (AuNPs) were synthesized following the method previously reported with minor modifications to accommodate different laboratory conditions [30]. To synthesize 15 nm AuNPs, 2.2 mM sodium citrate solution (150 mL) was taken in a dried three-necked flat-bottom flask and was heated to 100 °C under vigorous stirring. When the solution started to boil, 25.0 mM $HAuCl_4$ solution (1.0 mL) was added quickly and reacted for 10 min, until the solution changed from yellow to wine-colored. Synthesized nanoparticles (NPs) were used to fabricate LSPR sensor chips.

To synthesize 35 nm AuNPs, after the synthesis of 15 nm AuNPs and in the same flask, the solution was cooled to 90 °C. Then, 60.0 mM sodium citrate solution (1.0 mL) and 25.0 mM $HAuCl_4$ (1.0 mL) was added and reacted for 30 min. Synthesized NPs were used to fabricate LFIA strips. Fabricated AuNP size and morphology were analyzed using field-emission transmission electron microscopy (FE-TEM; JEM2100F, JEOL Ltd., USA), and the plasmon

absorbance peak was verified by UV–vis spectroscopy (V-770, JASCO International Co., Ltd., Japan).

2.3. LSPR sensor chip fabrication for ractopamine detection

We fabricated LSPR sensor chips following a previously reported method with minor modifications [31]. First, 5.0 × 0.8 cm glass substrate was subjected to ultrasonic treatment for 15 min in methanol to remove any surface impurities, then washed with distilled water several times. Cleaned substrates were soaked in 0.5% APTES (a linker to functionalize amines on the glass substrate) and reacted at 60.0 °C for 1 h. Amine-functionalized glass substrates were washed with distilled water at least five times to remove excess APTES, soaked in 15 nm AuNP solution, and reacted overnight at room temperature. Transparent wine-colored glass substrates were finally fabricated when AuNPs were successfully attached by self-assembly.

Ractopamine antibodies were fixed on AuNP surfaces to produce ractopamine-sensitive LSPR sensor chips. Pre-fabricated LSPR sensor chips were reacted with 600.0 μL RAC-Ab dissolved in phosphate buffer (PB), pH 7.4. RAC-Ab solutions were prepared at various concentrations (0, 0.001, 0.1, 1.0, 10.0, and 100.0 μg/mL) and used to verify optimum antibody concentration for detection. LSPR sensor chips were soaked at the optimized concentration and various reaction times (0, 5, 10, 15, 20, 25, and 30 min) to identify the optimum reaction time for antibody saturation. Results were analyzed with UV–vis spectroscopy, measuring absorbance over 400–700 nm to check peak shift for the LSPR sensor chip.

2.4. LFIA strip fabrication for ractopamine detection

We titrated 35 nm AuNPs to pH 9.0 using 0.25 M K_2CO_3 solution with various RAC-Ab quantities (0, 1.0, 1.5, and 2.0 μg/mL) on 5.0 mL AuNP solution and reacted in a rotator for 30 min at room temperature. Reacted solutions were centrifuged (6,000 rpm, 30 min, 4 °C) and the supernatant was removed to eliminate non-reacted antibodies. Subsequently, 1% BSA (blocking buffer), was added and reacted by rotator for 30 min to suppress non-specific reactions. The blocked solution was subsequently centrifuged (10,000 rpm, 15 min, 4 °C) and the supernatant was removed. Blocking and centrifugation were repeated twice, and RAC-Ab conjugated AuNPs were finally collected through phosphate buffer (PB) solution. Absorbance for bare and RAC-Ab conjugated AuNPs was measured using UV–vis spectroscopy to confirm the synthesis of RAC-Ab coated AuNPs.

Lateral flow immunoassay strips comprise an absorbent pad, NC membrane, conjugation pad, and sample pad. Conjugation pads, comprising glass fibers, were pretreated with 0.05% polyvinyl alcohol (PVA) and Tween 20 solution for 12 h, followed by drying overnight to remove non-specific binding before assembling LFIA sheets. RAC-Ab conjugated AuNPs were dropped on a completely dried conjugation pad and dried overnight at room temperature in a desiccator. Each 1.0 mg/mL anti-IgG and ractopamine-BSA was dispersed on NC membrane control (C) and test (T) lines, respectively, using the dispenser. Finally, the absorbent pad, NC membrane, conjugation pad, and sample pad were laminated on the backing card in regular sequence and then to 4.0 mm wide. Fabricated strips were kept at room temperature in a desiccator before use.

2.5. LSPR sensor chip and LFIA strip sensitivity to ractopamine

Fabricated LSPR sensor chips with optimized RAC-Ab concentration were reacted for 15 min with 600.0 μL various concentration ractopamine (1.0 fg/mL to 100.0 ng/mL) dissolved in 0.01 M PB with pH 7.4. Chips were then washed with PB, and LSPR peak intensity was analyzed by measuring absorbance between 400 − 700 nm using UV–vis spectroscopy. Fabricated LFIA strips were reacted for 10 min by soaking in 150.0 μL optimized running buffer with various ractopamine concentrations. Lines generated as the solution flowed were visually checked, and C and T line intensity for each concentration were photographed and analyzed using ImageJ software.

2.6. LSPR sensor chip and LFIA strips selectivity to ractopamine

To confirm ractopamine specificity and cross-reactivity for the developed LSPR sensor chips and LFIA strips, we crosschecked ractopamine detection and various interferences, including ractopamine analogs (epinephrine and clenbuterol), enrofloxacin, and creatine at 10 ng/mL. Peak shift was analyzed using UV–vis spectroscopy, and C and T line intensity after reaction with each interference solution using the ImageJ program.

2.7. Developed sensors applied to real pork samples

We used pork samples to check whether ractopamine could be detected in actual food. Pork samples purchased at the local mart were ground with a mixer, then 1.0 g homogenized pork samples were spiked with various ractopamine concentrations and stored at 4 °C for 1 h. Subsequently, 10.0 mL PB was mixed into the spiked pork samples, followed by centrifugation (8,000 rpm, 4 °C for 20 min), and supernatant (pork extract containing ractopamine in various concentrations) collected. We then reacted LSPR sensor chips and LFIA strips with pork extract using the detection process described above.

3. Results and discussion

3.1. LSPR sensor and LFIA strip ractopamine detection principle

Fig. 1 shows the fabrication and principal mechanism for ractopamine detection by LSPR sensor chips and LFIA strips. The LSPR sensor chip was coated with AuNPs on a glass substrate in a form that could be easily applied in the common cuvette. Antibodies were subsequently fixed to the LSPR sensor chip surface to functionalize it then the assembly was treated with ractopamine standard solution and spiked pork extract. Sensing performance

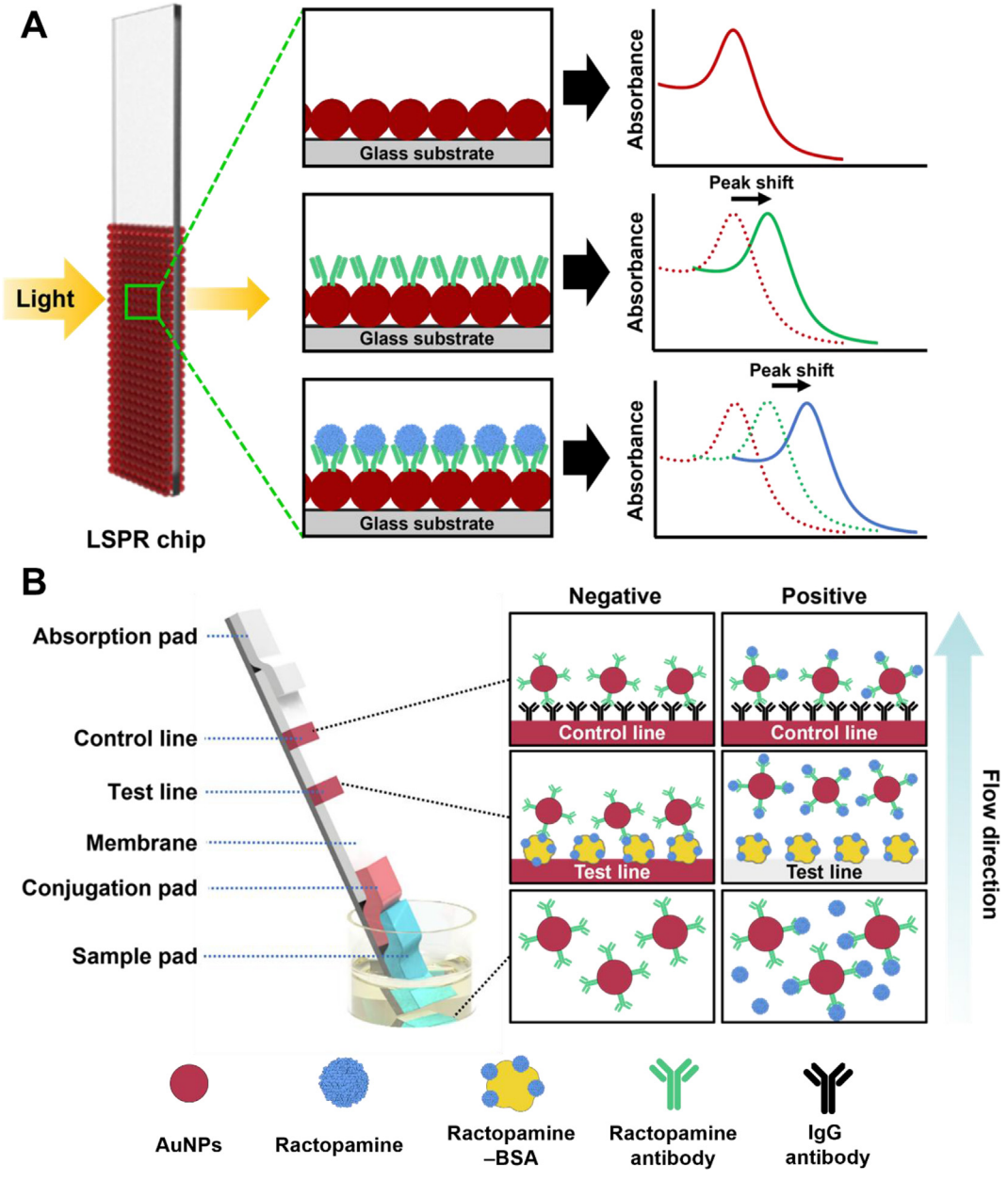

Fig. 1. Schematic illustration of LSPR sensor chip (A) and competitive LFIA strips (B) for detection of ractopamine.

was identified by LSPR peak shift induced by local refractive index changes due to biomolecular interactions at AuNP surfaces. Since these biomolecules have a higher refractive index than the buffer solution, molecular binding to AuNPs causes LSPR spectrum red-shift (Fig. 1A) [32].

The LFIA strips for this study were fabricated in a competitive assay format, which requires drying the antibody step at the sample site, accurate control over antibody quantity, and produces a consistent enhanced color signal proportional to antigen (ractopamine)-antibody (ractopamine specific antibody) response [33]. Ractopamine antibody conjugated AuNPs bind to ractopamine conjugated BSA immobilized on the T line. This binding site will only be free when there is no ractopamine in the test sample, hence the red T line is occurred and designated as the negative result. On the other hands, the positive result is shown by a competitive activity. When ractopamine existed in the pork sample, ractopamine competed with the immobilized ractopamine-BSA on T line with limited NP binding sites. Thus, T line is observed blurred red band or no band when ractopamine concentration contained high enough. With the sample continued to flow along the strip, the excess NP probe was combined with the anti-mouse IgG immobilized on C line, resulting in a red band. If the red C line is not observed, the test will be considered invalid [34,35]. Fig. 1B shows this mechanism. Very few sensors have been developed with AuNPs to detect food contaminants [7], hence the proposed sensors were highly efficient compared to others.

3.2. LSPR sensor chip and LFIA strips for ractopamine detection

3.2.1. Synthesized AuNPs characterization

We synthesized AuNPs from $HAuCl_4$ reduced by sodium citrate using the Turkevich/Frens reaction system. This nanomanufacturing method is highly reproducible, expedient, and cost-effective with low environmental impact [36], generating monodisperse, spherical, and surface functionalized AuNPs in aqueous solutions [36,37]. In particular, it was very important to synthesize specific-sized nanoparticles to improve biosensor performance, since AuNP size affects NP optical properties [38]. Previously studies have shown that smaller-sized AuNPs in LSPR sensor chips produced more hotspots that can change surface charge, resulting in more sensitive LSPR signals [39]; whereas it would be difficult to visually identify the detection area signal if the AuNPs are too small in the LFIA strip. For both cases, larger AuNPs (>50 nm) cause unstable antigen and antibody binding due to steric hindrance, and hence AuNP aggregation. Previous studies have identified that 30–40 nm AuNPs were highly effective [40,41]. Therefore, in this study, two sizes of AuNPs suitable for each sensor were synthesized and then characterized.

Fig. S1 shows that the AuNPs used to fabricate the LSPR sensor chip and LFIA strip sensor were characterized using FE-TEM and UV–vis spectra. AuNPs used for LSPR sensor chip production averaged 15.07 ± 1.72 nm (Fig. S1A, D); whereas AuNPs used for LFIA strips increased size by adding sodium citrate, to approximately 35.13 ± 3.74 nm (Fig. S1B, E). Synthesized AuNPs commonly have d-spacing ≈ 0.23 nm (Fig. S1C) consistent with Au (111) crystal plane [42]. AuNPs used for LSPR chip sensors and LFIA strips exhibited absorption peaks at 519 and 528 nm respectively, which were right-shifted as NP size increased (Fig. S1F) [43].

3.2.2. LSPR sensor chip optimization

Fig. 2 shows that synthesized 15 nm AuNPs were coated on the glass substrate surface followed by optimized antibody concentration and reaction time for antibodies to conjugate with the AuNPs to form antibody-functionalized LSPR sensor chips. Optimal antibody concentration was essential because the antibodies are the most important factor for immunosensor sensitivity and specificity [44].

Fig. 2A shows antibodies (1 ng/mL to 100 μg/mL) reacted with LSPR sensor chip. LSPR peak shift was measured to determine optimal concentration. The wavelength shift mechanism in LSPR is mainly based on analyte-surface binding interactions [45]. Although 1 μg/mL did not cause an observable peak shift, 10 μg/mL caused a significant peak shift. The peak shift for 100 μg/mL was 2.28 times higher than 10 μg/mL, but such high antibody concentration caused partial aggregation on the sensor chip surface, which can cause unstable assay conditions. Thus, approximately 10 μg/mL was the optimal antibody concentration for chip development.

Fig. 2B confirms optimal reaction time of 20 min for attaching the maximum antibody to the LSPR sensor chip surface and it was observed that as time increased, the LSPR peak increased significantly up to 20 min, but became saturated with no further significant changes over 20 min. Thus, the LSPR sensor chip to detect ractopamine was developed by reacting 10 μg/mL antibodies onto the glass strip coated with AuNPs for 20 min. Fig. 2C shows the optimized LSPR sensor chip reacted with ractopamine, confirming the UV–vis spectrum.

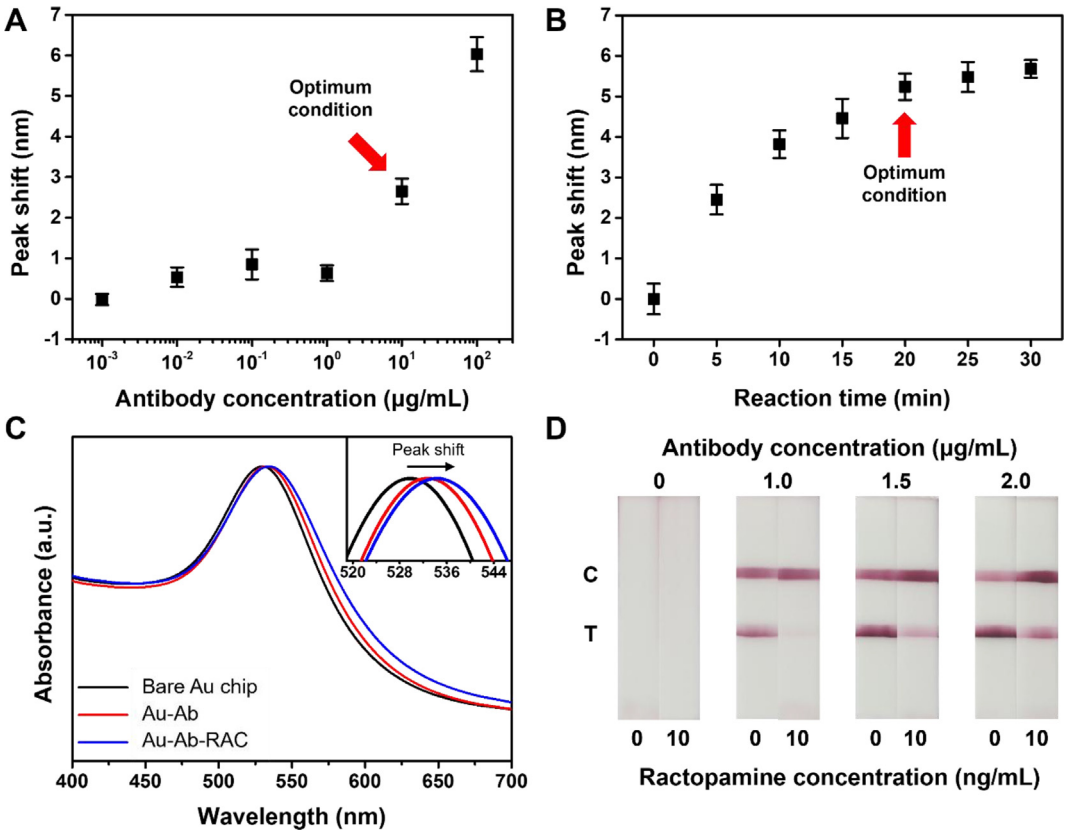

Fig. 2. Optimization of LSPR sensor chips and LFIA strips (A) Effect of the RAC-Ab with different concentrations (1 ng/mL–100 μg/mL) and (B) reaction time with 10 μg/mL of antibody for LSPR sensor chip (C) Detection of ractopamine using optimized LSPR sensor chip (D) Effect of the RAC-Ab with different concentrations for LFIA strips.

3.2.3. LFIA strip optimization

We wanted to develop LFIA strips to detect ractopamine using a competitive assay format. Therefore, we optimized antibody concentration conjugated to AuNPs, blocking buffers, and running buffers to improve assay sensitivity. Four different antibodies concentrations (0, 1.0, 1.5, and 2.0 μg/mL) were used and attached to AuNPs. Fig. S2A shows that AuNPs with attached antibodies exhibited red shifted in UV spectra due to refractive index changes on the particle surface, but the redshift did not differ significantly as antibody concentration increased. The control line tended to be visible, strong, and similar intensity for all strips reacted with 0–10 ng/mL ractopamine standard solution; whereas no line was visible in the absence of antibodies. Fig. 2D shows a strong T line occurred when no ractopamine was present (0 ng/mL), becoming more visible with increasing antibody concentration. However, the T line was highly indicated for positive ractopamine solution (10 ng/mL) and antibody concentration >1.5 μg/mL due to binding AuNPs conjugated antibodies to ractopamine-BSA immobilized to the T line. In contrast, the T line of 1.0 μg/mL antibody concentration was clear because all antibodies were saturated with ractopamine, leaving no free antigen-binding sites. Therefore, that the detection limit can be changed by varying antibody concentration, and detection sensitivity decreases with increasing antibody concentration. Therefore, we chose optimum antibody concentration = 1.0 μg/mL.

We also considered the effects of blocking and running buffers. Well-optimized blocking and running buffers are important LFIA parameters. The blocking buffer can reduce non-specific binding and hence improve detection sensitivity [26]. Antibody conjugated AuNPs were blocked using 10 mM PB, 10 mM phosphate buffer saline (PBS), and 20 mM Borate (pH 9.0) blocking buffers, each containing 1% BSA. Fig. S2B compares PB, PBS, and borate buffer effects for various ractopamine concentrations (0, 1, and 10 ng/mL). The blocking buffer made by 20 mM borate buffer enhanced T line intensity, creating a distinct visually detectable line. Fig. S2C shows optimization of NaCl concentration in running buffer. Generally, T line intensity increases with increasing NaCl concentration, but antibody conjugated AuNPs were not fully elevated and remained on membrane and conjugation pads at 300 mM NaCl. Therefore, we selected 150 mM as optimal

NaCl concentration for the running buffer considering the clean background and strong signal. These parameter optimizations helped develop sensors with acceptable reproducibility.

3.3. Sensitivity assay for LSPR sensor chip and LFIA strips using standard solutions

AuNPs on the glass slide surface self-assembled to fabricate the LSPR chip. As reported previously [46], this was mainly due to charge interaction between AuNP citric acids and amine groups on the functionalized glass chip [46]. The LSPR chip was functionalized by reacting 10 μg/mL antibodies for 20 min. PB with pH 7.4 was used to prepare ractopamine standard solution ranging from 1 fg/mL to 100 ng/mL that was subsequently reacted on specific chips.

Fig. 3A shows no significant peak shift for 1 fg/mL standard solution, but linear LSPR peak shift (R^2 = 0.9946) occurred as ractopamine increased from 10 fg/mL to 1 ng/mL. Limit of detection (LOD) for determining ractopamine by LSPR sensor chip was calculated as

$$LOD = k \times S_b/m, \quad (1)$$

where $k = 3$, corresponds to 98.3% confidence level; S_b is standard deviation from blank signal; and m is the calibration curve slope [47]. Thus, LOD = 1.19 fg/mL.

After optimizing antibody concentrations and reaction conditions, we verify sensitivity to ractopamine for the LFIA strip. There are two ways to express LOD for LFIA strips: visually or using calibrator equipment. Optimized running buffer was loaded with ractopamine concentrations 0, 0.5, 1, 5, 10, 25, 50, 75, and 100 ng/mL.

Fig. 3B shows that the T line is prominently visible up to 1 ng/mL, but significantly blurred for at 5 ng/mL and disappeared completely from 10 ng/mL. Thus, visually determined range for LFIA strips ≈ 0–10 ng/mL ractopamine and visible LOD (vLOD) = 5 ng/mL. Fig. S3 shows ractopamine detection results analyzed using the ImageJ program. Intensity ratios between the T and C lines were calculated by removing the background value. The LFIA strip achieved very narrow dynamic range ≈ 3–10 ng/mL (Fig. S3B) with linearity R^2 = 0.9968 and LOD = 2.27 ng/mL. Thus, LSPR and LFIA results verify that ractopamine can be successfully detected to USFDA residual tolerances.

3.4. Selectivity assay for LSPR sensor chip and LFIA strips

Food samples, such as pork, have very complex matrixes, which is a major factor that can affect ractopamine signal and sensor reliability [48]. Fig. 4 shows sensor selectivity for ractopamine was verified by monitoring detection results under various interferences (epinephrine, clenbuterol, enrofloxacin, and creatine) at 10 ng/mL concentration. Fig. 4B shows peak shift for LSPR sensor before and after 10 μg/mL antibody response to interferences. The peak shift for ractopamine was sharp, whereas the interferences exhibited a similar peak shift to the negative sample, i.e., no significant cross-reactivity was exhibited. Fig. 4C and D shows ractopamine interferences using optimized LFIA strips. Only samples with ractopamine did not show color on the T line, whereas the T line was always visible in the presence of interferences. Visual and ImageJ analysis confirmed similar results to negative samples. Therefore, the sensors developed in this study were sufficiently robust to binding and achieved high selectivity. Thus, the developed biosensors are suitable for detecting food contaminants in the field.

3.5. Real ractopamine sample detection

Pork samples spiked with various ractopamine concentrations were monitored to validate the fabricated optimized LSPR and LFIA devices' practicality for ractopamine detection and screening in

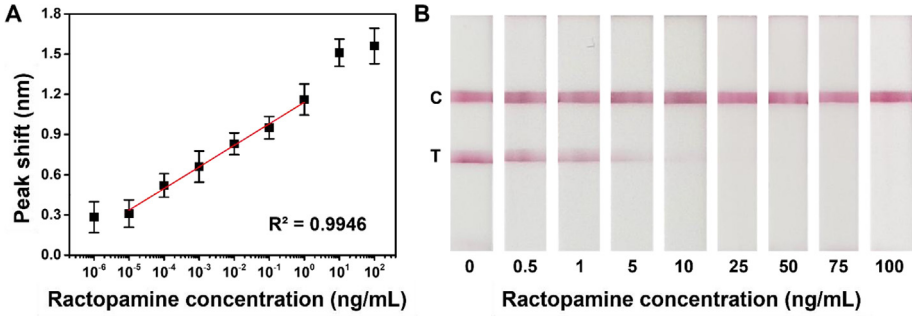

Fig. 3. Detection of ractopamine using (A) LSPR sensor chip and (B) LFIA strips with various concentrations of ractopamine standard solution.

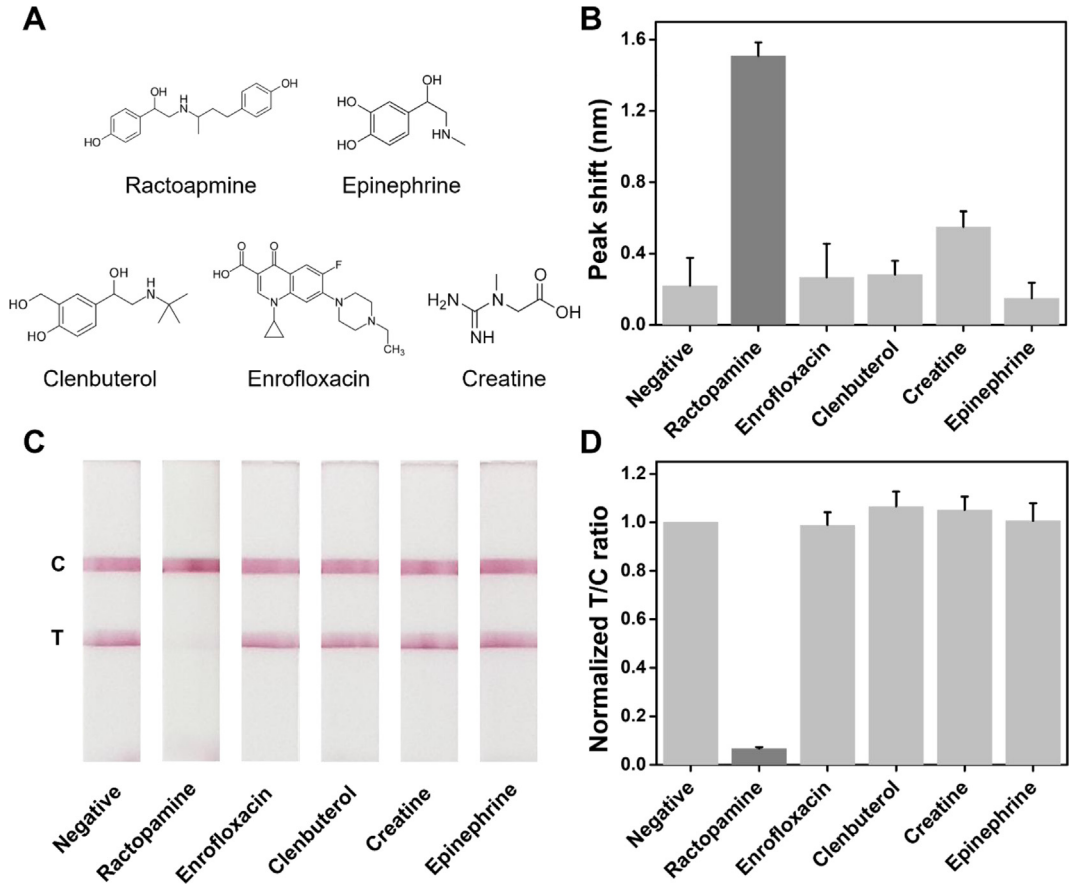

Fig. 4. Selectivity test to ractopamine and interferences at a concentration of 10 μg/mL (A) chemical structures of the ractopamine and interferences (B) LSPR peak shift response of LSPR sensor chip upon the addition of interferences (C) Image of the test strips with ractopamine and interferences, and (D) the normalized T/C ratio of LFIA strips produced by ImageJ program.

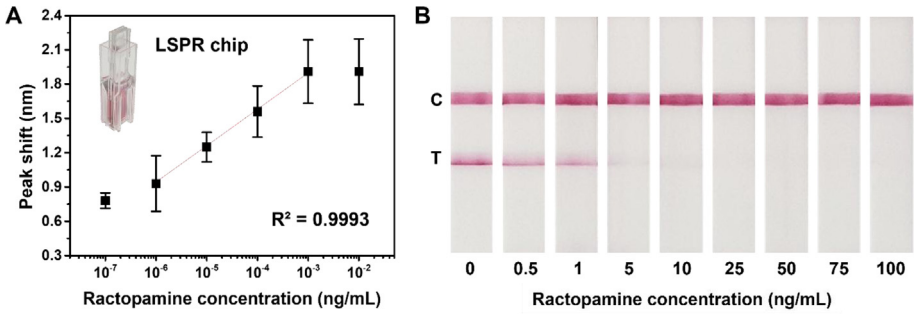

Fig. 5. Detection of ractopamine in pork extract using optimized LSPR sensor chip (A), and LFIA strips (B).

real samples. Fig. 5 shows that the LSPR sensor chip detected 0.1 fg/mL to 100 ng/mL, and the LFIA strips detected 0 ng/mL to 100 ng/mL ractopamine concentrations. Fig. 5A confirms LSPR sensor chip linearity $R^2 = 0.9993$ and LOD = 0.3 fg/mL within 1 fg/mL to 1 pg/mL ractopamine concentration. Table 1 shows excellent ractopamine recovery for three samples (93–108%). Previously developed sensors reported sensitivity at micro and nanogram levels [7],

Table 1. Result of the spike recovery test for the optimized LSPR sensor chip.

Spiked (ng/mL)	Detected (ng/mL)	Recovery[a] (%)	RSD[b] (%, n = 5)
4.0×10^{-6}	3.72×10^{-6}	108	22.2
5.0×10^{-5}	5.10×10^{-5}	98	14.1
2.5×10^{-4}	2.71×10^{-4}	92	13.8

[a] Recovery (%) = Detected/Spiked × 100.
[b] RSD, Relative standard deviation (%) = SD/mean × 100.

Table 2. Comparison of different methods used to determine ractopamine.

Method	Sample	LOD	Linear range	Reference
QuEChERS/LC-MS	Pork	1.5 μg/kg	2.5–20 μg/kg	[11]
HPLC	Beef	0.01 μg/mL	0.05–2.5 μg/mL	[49]
GC–MS	Swine liver and urine	0.5 ng/mL	–	[13]
ELISA	Chicken, Swine, Pettitoes	0.35 ng/mL	2–512 ng/mL	[50]
SPR	Swine urine	0.09 ng/mL	0.3–32 ng/mL	[51]
Chemiluminescent (CL) based LFIA	Swine urine	0.20 ng/mL	0.50–40 ng/mL	[52]
Colorimetric	Swine feed	0.003 ng/mL	0.03–150 ng/mL	[53]
LSPR	Pork	1.19 fg/mL	10 fg/mL – 1 ng/mL	This work
LFIA	Pork	2.27 ng/mL	3–10 ng/mL	This work

whereas the proposed sensor achieves sensitivity at pico and femtogram levels. Thus, the developed sensor is highly sensitive, portable, and can detect a diverse range of food contaminants in pork meat. Fig. 5B shows LFIA strips results after reacting with ractopamine spiked pork samples for 10 min, achieving vLOD ≈5 ng/mL. However, the analysis is difficult due to the very narrow linear range as discussed above regarding quantitative analysis using LFIA strips. These results confirm that both sensors can detect ractopamine as sensitively as a standard solution in real samples. Table 2 compares detection levels for previously reported sensors with the proposed sensor developed in this study.

4. Conclusion

Veterinary drugs administered in food-producing animals generate drug residues in all the animal-derived food products that pose potential health hazards to consumers. The immuno-colloidal AuNPs-based LSPR sensor chip and LFIA strips developed here will be highly beneficial to detect ractopamine, as a model drug residue, in pork meat samples on-site with significant sensing performance. The LSPR sensor chip achieved very low LOD = 1.19 fg/mL, whereas the LFIA strip achieved LOD = 2.27 ng/mL. The LSPR sensor chip exhibited sensitivity of 4.20×10^6 times larger than LFIA, detect very low ractopamine concentration in approximately 30 min whereas the LFIA strip detects narrow range of ractopamine with the naked eye in just 5–10 min. The two sensors are complementarily able to rule out each other's shortcomings perfectly and also overcomes limitations such as sensitivity and requirement of more precise analysis systems lending it to be used as field inspection sensor. Both sensors detect and screen ractopamine with sensitivity sufficiently cover USFDA ractopamine residual tolerances. We expect that the developed sensor will open many innovative approaches and advance the fabrication of on-site sensors to detect specific food additives.

Conflict of interest

The authors declare that they have no conflict of interest.

Acknowledgments

This work was carried out with the support of the "Cooperative Research Program for Agriculture Science and Technology Development (Project No. PJ01423804)" Rural Development Administration, Republic of Korea.

Appendix

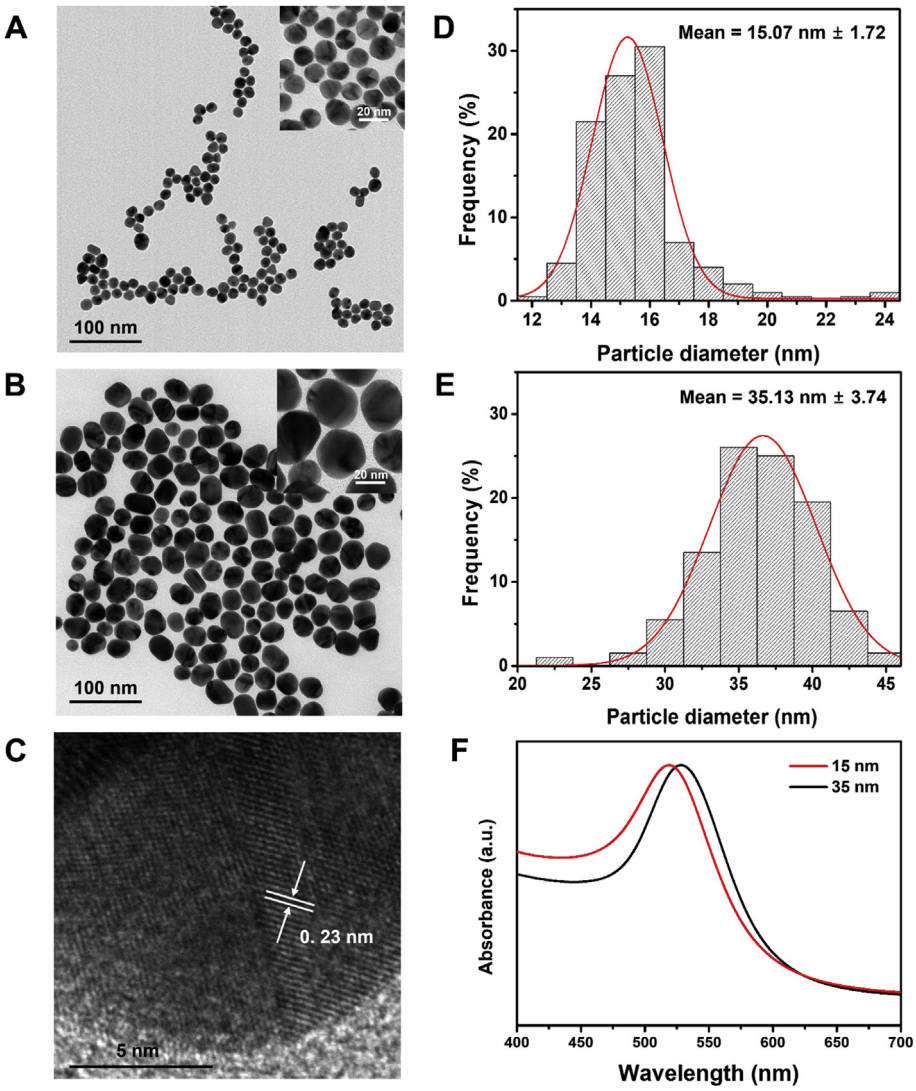

Fig. S1. Characterization of AuNPs. (A, D) FE-TEM analysis and size histogram of 15 nm AuNPs, and (B, E) 35 nm of AuNPs. (C) Crystalline planes (111) corresponding to a gold FCC structure. (F) UV-vis absorbance spectra of 15 nm and 35 nm AuNPs.

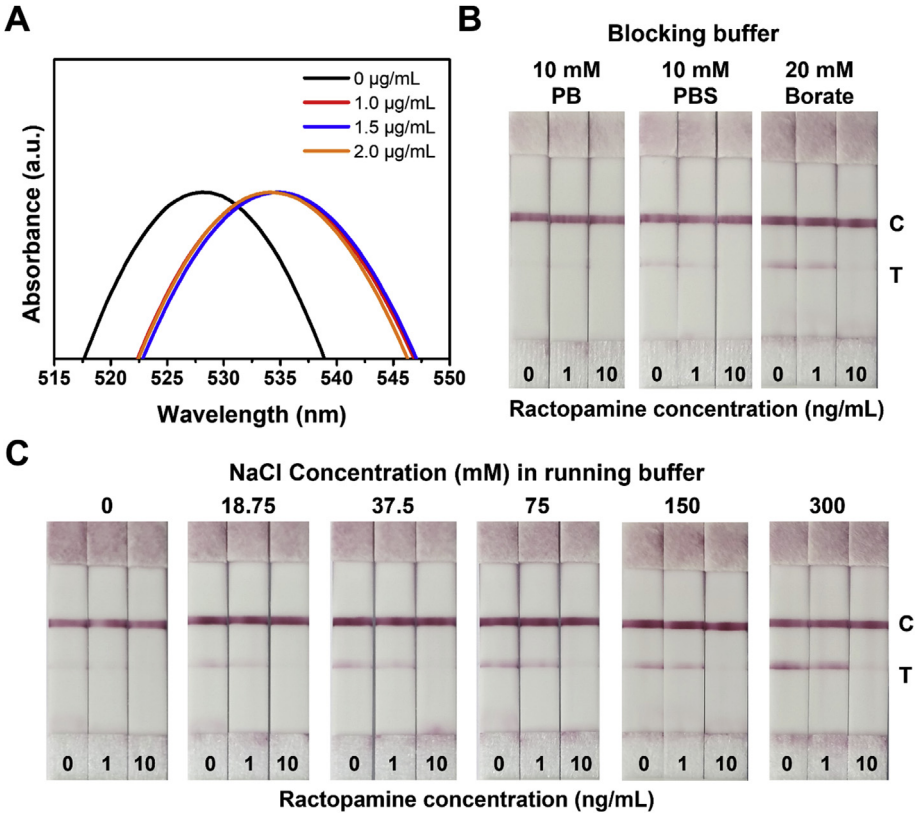

Fig. S2. Optimization of LFIA strip for detection of ractopamine. (A) UV-vis spectrum of anti-ractopamine conjugated AuNPs. (B) Effect of the various type of blocking buffer. (C) Effect of the NaCl concentration in running buffer.

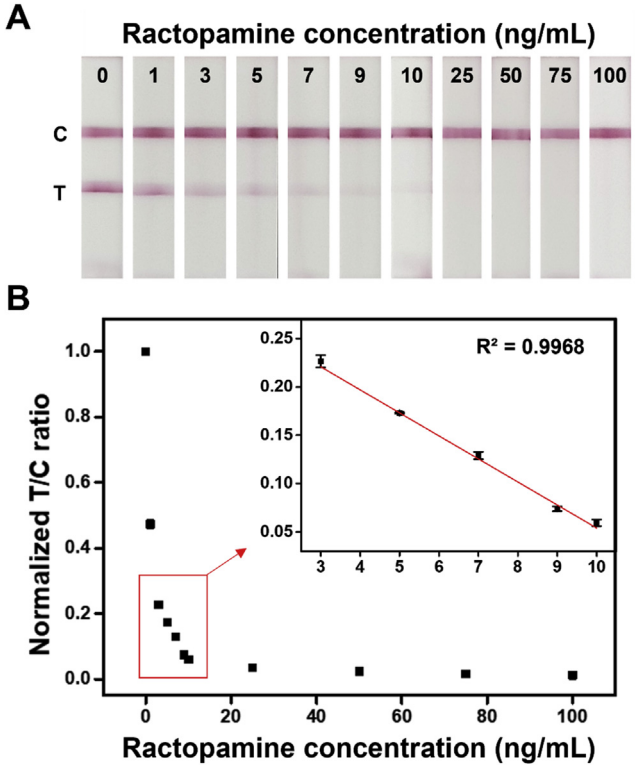

Fig. S3. (A) Image of the LFIA strips with the increasing ractopamine concentration. (B) Relationship between normalized T/C ratio and the ractopamine concentration. The T/C ratio was calculated by T line intensity over C line intensity. T and C line intensity was measured using the ImageJ program.

References

[1] Baker P, Friel S. Food systems transformations, ultra-processed food markets and the nutrition transition in Asia. Glob Health 2016;12:80.

[2] Hannah R, Max R. Meat and dairy production. 2017. Available at: https://ourworldindata.org/meat-production.

[3] Beyene T. Veterinary drug residues in food-animal products: its risk factors and potential effects on public health. J Vet Sci Technol 2016;7:1–7.

[4] Wang X, Wang K-w, Xu Z-z, Yang S-m, Zhao Y. Development and validation of a multi-residue analytical method for veterinarian and human pharmaceuticals in livestock urine and blood using UHPLC-QTOF. J Chromatogr B Biomed Appl 2021;1167:122564.

[5] Tufa T. Veterinary drug residues in food-animal products: its risk factors and potential effects on public health. J Vet Sci Technol 2015;7.

[6] Wang B, Xie K, Lee K. Veterinary drug residues in animal-derived foods: sample preparation and analytical methods. Foods 2021;10:555.

[7] Gaudin V. Chapter 11 - receptor-based electrochemical biosensors for the detection of contaminants in food products. In: Ensafi AA, editor. Electrochemical biosensors. Elsevier; 2019. p. 307–65.

[8] Wang C, Li X, Yu F, Wang Y, Ye D, Hu X, et al. Multi-class analysis of veterinary drugs in eggs using dispersive-solid phase extraction and ultra-high performance liquid chromatography-tandem mass spectrometry. Food Chem 2021;334:127598.

[9] Peltomaa R, Benito-Peña E, Gorris HH, Moreno-Bondi MC. Biosensing based on upconversion nanoparticles for food quality and safety applications. Analyst 2021;146:13–32.

[10] Freire EF, Borges KB, Tanimoto H, Nogueira RT, Bertolini LC, de Gaitani CM. Development and validation of a simple method for routine analysis of ractopamine hydrochloride in raw material and feed additives by HPLC. J AOAC Int 2009;92:757–64.

[11] Valese AC, Oliveira GAP, Kleemann CR, Molognoni L, Daguer H. A QuEChERS/LC–MS method for the analysis of ractopamine in pork. J Food Compos Anal 2016;47:38–44.

[12] Shelver WL, Smith DJ. Development of an immunoassay for the β-adrenergic agonist ractopamine. J Immunoassay 2000;21:1–23.

[13] Wang JP, Li XW, Zhang W, Shen JZ. Development of immunoaffinity sample-purification for GC–MS analysis of ractopamine in swine tissue. Chromatographia 2006;64:613–7.

[14] Kumar Y, Narsaiah K. Rapid point-of-care testing methods/devices for meat species identification: a review. Compr Rev Food Sci Food Saf 2021;20:900–23.

[15] Nguyen QH, Kim MI. Using nanomaterials in colorimetric toxin detection. Biochip J 2021;15:123–34.

[16] Kim T-Y, Lim JW, Lim M-C, Song N-E, Woo M-A. Aptamer-based fluorescent assay for simple and sensitive detection of fipronil in liquid eggs. Biotechnol Bioproc E 2020;25:246–54.

[17] Kasetsirikul S, Shiddiky MJ, Nguyen N-T. Challenges and perspectives in the development of paper-based lateral flow assays. Microfluid Nanofluidics 2020;24:1–18.

[18] Chang C-C, Chen C-P, Wu T-H, Yang C-H, Lin C-W, Chen C-Y. Gold nanoparticle-based colorimetric strategies for chemical and biological sensing applications. Nanomaterials 2019;9.

[19] Hua Z, Yu T, Liu D, Xianyu Y. Recent advances in gold nanoparticles-based biosensors for food safety detection. Biosens Bioelectron 2021;179:113076.

[20] Jiang N, Ahmed R, Damayantharan M, Ünal B, Butt H, Yetisen AK. Lateral and vertical flow assays for point-of-care Diagnostics. Adv Healthc Mater 2019;8:1900244.

[21] Khlebtsov B, Khlebtsov N. Surface-enhanced Raman scattering-based lateral-flow immunoassay. Nanomaterials 2020;10:2228.

[22] Sepúlveda B, Angelomé PC, Lechuga LM, Liz-Marzán LM. LSPR-based nanobiosensors. Nano Today 2009;4:244–51.

[23] Willets KA, Van Duyne RP. Localized surface plasmon resonance spectroscopy and sensing. Annu Rev Phys Chem 2007;58:267–97.

[24] Wang Y, Zhou J, Li J. Construction of plasmonic nanobiosensor-based devices for point-of-care testing. Small Methods 2017;1:1700197.

[25] Chen J-S, Chen P-F, Lin HT-H, Huang N-T. A Localized surface plasmon resonance (LSPR) sensor integrated automated microfluidic system for multiplex inflammatory biomarker detection. Analyst 2020;145:7654–61.

[26] Zhan L, Granade T, Liu Y, Wei X, Youngpairoj A, Sullivan V, et al. Development and optimization of thermal contrast amplification lateral flow immunoassays for ultrasensitive HIV p24 protein detection. Microsyst Nanoeng 2020;6:54.

[27] Raeisossadati MJ, Danesh NM, Borna F, Gholamzad M, Ramezani M, Abnous K, et al. Lateral flow based immunobiosensors for detection of food contaminants. Biosens Bioelectron 2016;86:235–46.

[28] Aroeira CN, Feddern V, Gressler V, Molognoni L, Daguer H, Dalla Costa OA, et al. Determination of ractopamine residue in tissues and urine from pig fed meat and bone meal. Food Addit Contam 2019;36:424–33.

[29] Meeting JFWECoFA. Residue evaluation of certain veterinary drugs: joint FAO/WHO expert committee on food additives, 66th meeting 2006. Food & Agriculture Org.; 2006.

[30] BastúS NG, Comenge J, Puntes VC. Kinetically controlled seeded growth synthesis of citrate-stabilized gold nanoparticles of up to 200 nm: size focusing versus ostwald ripening. Langmuir 2011;27:11098–105.

[31] Oh SY, Heo NS, Bajpai VK, Jang S-C, Ok G, Cho Y, et al. Development of a cuvette-based LSPR sensor chip using a plasmonically active transparent strip. Front Bioeng Biotechnol 2019;7.

[32] Anker JN, Hall WP, Lyandres O, Shah NC, Zhao J, Van Duyne RP. Biosensing with plasmonic nanosensors. Nat Mater 2008;7:442–53.

[33] Sun Y, Yang S, Yang J, Hu X, Wei Q, Wang Y, et al. An accurate and amplifying competitive lateral flow immunoassay for the sensitive detection of haptens. Food Agric Immunol 2021;32:766–77.

[34] Wong R, Tse H. Lateral flow immunoassay. Springer Science & Business Media; 2008.

[35] Bong J-H, Kim T-H, Jung J, Lee SJ, Sung JS, Lee CK, et al. Competitive immunoassay of SARS-CoV-2 using pig sera-derived anti-SARS-CoV-2 antibodies. Biochip J 2021;15:100–8.

[36] Larm NE, Essner JB, Pokpas K, Canon JA, Jahed N, Iwuoha EI, et al. Room-temperature Turkevich method: formation of gold nanoparticles at the speed of mixing using cyclic oxocarbon reducing agents. J Phys Chem C 2018;122:5105–18.

[37] Kettemann F, Birnbaum A, Witte S, Wuithschick M, Pinna N, Kraehnert R, et al. Missing piece of the mechanism of the Turkevich method: the critical role of citrate protonation. Chem Mater 2016;28:4072–81.

[38] Toubanaki DK, Margaroni M, Prapas A, Karagouni E. Development of a nanoparticle-based lateral flow strip biosensor for visual detection of whole nervous necrosis virus particles. Sci Rep 2020;10:1–12.

[39] Kim J, Oh SY, Shukla S, Hong SB, Heo NS, Bajpai VK, et al. Heteroassembled gold nanoparticles with sandwich-immunoassay LSPR chip format for rapid and sensitive detection of hepatitis B virus surface antigen (HBsAg). Biosens Bioelectron 2018;107:118–22.

[40] Khlebtsov BN, Tumskiy RS, Burov AM, Pylaev TE, Khlebtsov NG. Quantifying the numbers of gold nanoparticles in the test zone of lateral flow immunoassay strips. ACS Appl Nano Mater 2019;2:5020–8.

[41] Toubanaki DK, Margaroni M, Prapas A, Karagouni E. Development of a nanoparticle-based lateral flow strip

biosensor for visual detection of whole nervous necrosis virus particles. Sci Rep 2020;10:6529.
[42] Shi Y, Huang J-K, Jin L, Hsu Y-T, Yu SF, Li L-J, et al. Selective decoration of Au nanoparticles on monolayer MoS2 single crystals. Sci Rep 2013;3:1839.
[43] Haiss W, Thanh NTK, Aveyard J, Fernig DG. Determination of size and concentration of gold nanoparticles from UV–Vis spectra. Anal Chem 2007;79:4215–21.
[44] Preechakasedkit P, Siangproh W, Khongchareonporn N, Ngamrojanavanich N, Chailapakul O. Development of an automated wax-printed paper-based lateral flow device for alpha-fetoprotein enzyme-linked immunosorbent assay. Biosens Bioelectron 2018;102:27–32.
[45] Valcárcel M, López-Lorente A. Gold nanoparticles in analytical chemistry. 2014.
[46] Zheng J, Zhu Z, Chen H, Liu Z. Nanopatterned assembling of colloidal gold nanoparticles on silicon. Langmuir 2000;16: 4409–12.
[47] Á Lavín, Vicente JD, Holgado M, Laguna MF, Casquel R, Santamaría B, et al. On the determination of uncertainty and limit of detection in label-free biosensors. Sensors 2018;18:2038.
[48] Liang X, Song X, Wang Z, Zhang Q. Evaluation of different food matrices via a dihydropteroate synthase-based biosensor for the screening of sulfonamide residues. Food Agric Immunol 2020;31:352–66.
[49] Gao T, Ye N, Li J. Determination of ractopamine and clenbuterol in beef by graphene oxide hollow fiber solid-phase microextraction and high-performance liquid chromatography. Anal Lett 2016;49:1163–75.
[50] Zhang Y, Wang F, Fang L, Wang S, Fang G. Rapid determination of ractopamine residues in edible animal products by enzyme-linked immunosorbent assay: development and investigation of matrix effects. J Biomed Biotechnol 2009; 2009:579175.
[51] Wang S, Zhao S, Wei X, Zhang S, Liu J, Dong Y. An improved label-free indirect competitive SPR immunosensor and its comparison with conventional ELISA for ractopamine detection in swine urine. Sensors 2017;17:604.
[52] Gao H, Han J, Yang S, Wang Z, Wang L, Fu Z. Highly sensitive multianalyte immunochromatographic test strip for rapid chemiluminescent detection of ractopamine and salbutamol. Anal Chim Acta 2014;839:91–6.
[53] Zhou Y, Wang P, Su X, Zhao H, He Y. Colorimetric detection of ractopamine and salbutamol using gold nanoparticles functionalized with melamine as a probe. Talanta 2013;112: 20–5.